Inter-comparison of hemispherical conical reflectance factors (HCRF) measured with four fibre-based spectrometers

K. Anderson,[1,*] M. Rossini,[2] J. Pacheco-Labrador,[3] M. Balzarolo,[4] A. Mac Arthur,[5] F. Fava,[2] T. Julitta,[2] and L. Vescovo[6]

[1] *Environment and Sustainability Institute, University of Exeter, Cornwall Campus, TR109EZ, UK*
[2] *Remote Sensing of Environmental Dynamics Laboratory, DISAT, Università degli Studi Milano-Bicocca, Piazza della Scienza 1, 20126 Milan, Italy*
[3] *Environmental Remote Sensing and Spectroscopy Laboratory (SpecLab), CCHS—CSIC, C/Albasanz 26-28, Madrid 28037, Spain*
[4] *Dipartimento per la Innovazione nei sistemi Biologici, Agroalimentari e Forestali, DIBAF, Università della Tuscia, Via S.C. de Lellis, 01100 Viterbo, Italy*
[5] *Natural Environment Research Council, Field Spectroscopy Facility, University of Edinburgh, UK*
[6] *Centro Ecologia Alpina, Fondazione Edmund Mach, Viote del Monte Bondone, Trento, Italy*
[*] *Karen.Anderson@exeter.ac.uk*

Abstract: We describe the results of an experiment designed to compare the radiometric performance of four different spectroradiometers in ideal field conditions. A carefully designed experiment where instruments were simultaneously triggered was used to measure the Hemispherical Conical Reflectance Factors (HCRF) of four targets of varying reflectance. The experiment was in two parts. Stage 1 covered a 2 hour period finishing at solar noon, where 50 measurements of the targets were collected in sequence. Stage 2 comprised 10 rapid sequential measurements over each target. We applied a method for normalising full width half maximum (FWHM) differences between the instruments, which was a source of variability in the raw data. The work allowed us to determine data reproducibility, and we found that lower-cost instruments (Ocean Optics and PP Systems) produced data of similar radiometric quality to those manufactured by Analytical Spectral Devices (ASD –here we used the ASD FieldSpec Pro) in the spectral range 400-850 nm, which is the most significant region for research communities interested in measuring vegetation dynamics. Over the longer time-series there were changes in HCRF caused by the structural and spectral characteristics of some targets.

OCIS codes: (280.0280) Remote sensing and sensors; (280.4788) Optical sensing and sensors.

References and links

1. T. Hilker, N. C. Coops, S. B. Coggins, M. A. Wulder, M. Brown, T. A. Black, Z. Nesic, and D. Lessard, "Detection of foliage conditions and disturbance from multi-angular high spectral resolution remote sensing," Remote Sens. Environ. **113**(2), 421–434 (2009).
2. T. Hilker, N. C. Coops, Z. Nesic, M. A. Wulder, and A. T. Black, "Instrumentation and approach for unattended year round tower based measurements of spectral reflectance," Comput. Electron. Agric. **56**(1), 72–84 (2007).
3. J. A. Gamon, Y. Cheng, H. Claudio, L. MacKinney, and D. A. Sims, "A mobile tram system for systematic sampling ecosystem optical properties," Remote Sens. Environ. **103**(3), 246–254 (2006).
4. M. Meroni, A. Barducci, S. Cogliati, F. Castagnoli, M. Rossini, L. Busetto, M. Migliavacca, E. Cremonese, M. Galvagno, R. Colombo, and U. M. di Cella, "The hyperspectral irradiometer, a new instrument for long-term and unattended field spectroscopy measurements," Rev. Sci. Instrum. **82**(4), 043106 (2011).
5. M. Rossini, S. Cogliati, M. Meroni, M. Migliavacca, M. Galvagno, L. Busetto, E. Cremonese, T. Julitta, C. Siniscalco, U. Morra di Cella, and R. Colombo, "Remote sensing-based estimation of gross primary production in a subalpine grassland," Biogeosci. **9**(7), 2565–2584 (2012).

#174520 - $15.00 USD Received 22 Aug 2012; revised 2 Nov 2012; accepted 4 Nov 2012; published 7 Jan 2013

6. J. A. Gamon, L. Serrano, and J. S. Surfus, "The photochemical reflectance index: an optical indicator of photosynthetic radiation use efficiency across species, functional types, and nutrient levels," Oecologia **112**(4), 492–501 (1997).
7. P. J. Zarco-Tejada, V. Gonzalez-Dugo, and J. A. J. Berni, "Fluorescence, temperature and narrow-band indices acquired from a UAV platform for water stress detection using a micro-hyperspectral imager and a thermal camera," Remote Sens. Environ. **117**, 322–337 (2012).
8. M. Meroni, M. Rossini, L. Guanter, L. Alonso, U. Rascher, R. Colombo, and J. Moreno, "Remote sensing of solar induced chlorophyll fluorescence: review of methods and applications," Remote Sens. Environ. **113**(10), 2037–2051 (2009).
9. M. Rossini, M. Meroni, M. Migliavacca, G. Manca, S. Cogliati, L. Busetto, V. Picchi, A. Cescatti, G. Seufert, and R. Colombo, "High resolution field spectroscopy measurements for estimating gross ecosystem production in a rice field," Agric. For. Meteorol. **150**(9), 1283–1296 (2010).
10. M. Balzarolo, K. Anderson, C. Nichol, M. Rossini, L. Vescovo, N. Arriga, G. Wohlfahrt, J.-C. Calvet, A. Carrara, S. Cerasoli, S. Cogliati, F. Daumard, L. Eklundh, J. A. Elbers, F. Evrendilek, R. N. Handcock, J. Kaduk, K. Klumpp, B. Longdoz, G. Matteucci, M. Meroni, L. Montagnani, J.-M. Ourcival, E. P. Sánchez-Cañete, J.-Y. Pontailler, R. Juszczak, B. Scholes, and M. P. Martín, "Ground-Based Optical Measurements at European Flux Sites: A Review of Methods, Instruments and Current Controversies," Sensors (Basel) **11**(8), 7954–7981 (2011).
11. G. Schaepman-Strub, M. E. Schaepman, T. H. Painter, S. Dangel, and J. V. Martonchik, "Reflectance quantities in optical remote sensing–definitions and case studies," Remote Sens. Environ. **103**(1), 27–42 (2006).
12. K. Anderson, J. L. Dungan, and A. MacArthur, "On the reproducibility of field measured reflectance factors in the context of vegetation studies," Remote Sens. Environ. **115**(8), 1893–1905 (2011).
13. K. L. Castro-Esau, G. A. Sanchez-Azofeifa, and B. Rivard, "Comparison of spectral indices obtained using multiple spectroradiometers," Remote Sens. Environ. **103**(3), 276–288 (2006).
14. M. Morys, F. M. Mims III, S. Hagerup, S. E. Anderson, A. Baker, J. Kia, and T. Walkup, "Design, calibration, and performance of MICROTOPS II handheld ozone monitor and Sun photometer," J. Geophys. Res. **106**(D13), 14573–14582 (2001).
15. A. Damm, A. Erler, W. Hillen, M. Meroni, M. E. Schaepman, W. Verhoef, and U. Rascher, "Modeling the impact of spectral sensor configurations on the FLD retrieval accuracy of sun-induced chlorophyll fluorescence," Remote Sens. Environ. **115**(8), 1882–1892 (2011).
16. M. Meroni, L. Busetto, L. Guanter, S. Cogliati, G. F. Crosta, M. Migliavacca, C. Panigada, M. Rossini, and R. Colombo, "Characterization of fine resolution field spectrometers using solar Fraunhofer lines and atmospheric absorption features," Appl. Opt. **49**(15), 2858–2871 (2010).
17. E. M. Rollin, E. J. Milton, and D. R. Emery, "Reference panel anisotropy and diffuse radiation - some implications for field spectroscopy," Int. J. Remote Sens. **21**(15), 2799–2810 (2000).
18. M. Wettle, V. E. Brando, and A. G. Dekker, "A methodology for retrieval of environmental noise equivalent spectra applied to four Hyperion scenes of the same tropical coral reef," Remote Sens. Environ. **93**(1-2), 188–197 (2004).
19. J. A. Gamon, J. Peñuelas, and C. B. Field, "A narrow waveband spectral index that tracks diurnal changes in photosynthetic efficiency," Remote Sens. Environ. **41**(1), 35–44 (1992).

1. Introduction

Measurements of reflectance quantities at eddy covariance sites are increasingly relying on hyperspectral instrumentation [1–5] because narrowband spectral indices are good proxies for plant physiological processes such as the xanthophyll cycle (e.g. photochemical reflectance index, PRI [6]), or sun-induced chlorophyll fluorescence [7–9]. Hyperspectral spectroradiometers are complex devices and there are a great range of models on offer [10] each with varying optical characteristics and operating modes. Several studies have commented on the importance of quantifying the reproducibility of field measurements of spectral reflectance measured using such systems [11–13]. Despite the fact that these instruments are increasingly being utilised in operational settings, and that there is a strong need for measurements to be cross-comparable across different sites, there is very little published work demonstrating whether data show good reproducibility [10]. This is particularly true for the new generation of lightweight, miniaturised spectroradiometers (e.g. those manufactured by companies such as Ocean Optics and PP Systems) which are compact enough to be easily deployed across eddy covariance sites in a cost-effective manner. In particular, the network of eddy covariance towers across Europe overseen by the Integrated Carbon Observation System (ICOS; http://www.icos-infrastructure.eu/) is calling for input from the hyperspectral measurement community about which systems are best suited to deployment on flux towers. Before such advice can be provided, information is needed about the relative radiometric performance of the different systems available. This paper provides a

#174520 - $15.00 USD Received 22 Aug 2012; revised 2 Nov 2012; accepted 4 Nov 2012; published 7 Jan 2013

first field-based quantitative assessment of the reproducibility of hemispherical conical reflectance factors (HCRF) measured by four individual fibre-optic based hyperspectral spectroradiometers, including three miniaturised systems (two from Ocean Optics (http://www.oceanoptics.com/) and one from PP Systems (http://www.ppsystems.com/)) that have already been shown to be ideally suited to deployment at eddy covariance sites [2, 4, 5].

2. Methodology

2.1 Spectroradiometers

Four individual spectroradiometers participated in the inter-comparison experiment. All of these instruments were fibre-optic instruments and are described in Table 1. Note that both the Ocean Optics Vis-NIR and Ocean Optics NIR Fluorescence instruments are component parts of the "Hyperspectral Irradiometer" [4, 5] and in this experiment they were operated within a Peltier thermally regulated box (model NT-16, Magapor, Zaragoza, Spain) keeping the internal temperature at 25°C in order to avoid temperature-dependent drifts in sensitivity. The ASD FieldSpec Pro and PP Systems Unispec spectroradiometer were not buffered against temperature changes in the experiment.

Table 1. Details of spectroradiometers participating in the experiment.

Instrument name	Operating range	FWHM in centre of detector array	Serial number	Owner/operator
PP Systems Unispec	310-1100	10 nm	2038	CSIC, Spain
Ocean Optics Vis-NIR	350-1050 nm	1 nm	HR4C1078	University of Milano Bicocca, Italy
Ocean Optics NIR fluorescence	720-800 nm	0.15 nm	HR4C1076	
ASD FieldSpec Pro	350-2500 nm*	3 nm	6354/2	Fondatione Edmund Mach, Italy

***** Note that we report only on data from detector 1: Vis-NIR silicon photodiode array (range 350–1050 nm) in this paper.

2.2 Experimental approach

The experiment was performed in an open meadow at Monte Bondone, Italy (46.015°N,11.054°E) on 11 July 2011. The spectrometers were configured so that the measurements being collected were as comparable as possible given the different physical system arrangements, and their capabilities in field conditions. Spectrum averaging was set to a common value of 4. All spectrometers were operated with bare fibre optics where the field-of-view was between 21 and 25 degrees (depending on the instrument used, and according to manufacturer's specifications). A specially designed rotating tripod arm with a fibre optic holder was used to ensure that the fibres of each instrument were as close together as possible – there was less than 3 mm separation between the fibre positions on the rotating tripod arm. This meant that the four instruments were measuring as similar a spatial area on the targets of interest as could be physically achieved (Fig. 1). The rotating tripod arm could be moved with an angular precision of 1 degree in the azimuthal plane to ensure that the foreoptics were pointing at the same positions on each target for each measurement. The azimuthal angles at which measurements were collected were pre-defined before the experiment started allowing reproducible positioning with each circuit of measurements. The height of the tripod arm above the measurement surfaces was fixed at an average distance of 23.6 cm throughout, and vertical positioning precision was perfect because the rotating arm was locked in place in this domain. The clocks on the instrument computers were sychronised according to GPS time so that data could be easily matched, and accurate log sheets of filenames were kept by all instrument operators during the experiment. The integration time of the sensors was the only factor that could not be set to a standard level across all instruments because of their variable dynamic radiometric sensitivities – doing so would have caused some sensors to saturate,

#174520 - $15.00 USD Received 22 Aug 2012; revised 2 Nov 2012; accepted 4 Nov 2012; published 7 Jan 2013

whilst others would have been poorly optimised for a particular set of field conditions. Given our focus on assessing the field-based reproducibility of HCRFs at eddy covariance sites, we decided it was methodologically sound to "simulate" the real conditions of operational deployment in the field, and in reality this necessitated the use of varying integration speeds across the different instruments.

Four target surfaces were measured using the instruments (Fig. 1) and these targets were placed upon an optically black cloth background to ensure minimal scattering from nearby objects (not shown in Fig. 1 for clarity of presentation):

1. 99% Spectralon panel ("reference") – serial number 24414
2. 75% Spectralon panel ("grey75") – serial number OD19D SRT # 036
3. 20% Spectralon panel ("grey20") – serial number 4240D SRT# 036
4. Grassland target ("grass") with a plant area index of 3.41 m^2 m^{-2} (determined by destructive sampling of the leaves and stems after the experiment) and total biomass weight of 133.65 g m^{-2}

The experiment began at 0855 local time. The experiment had two stages, described below:

Stage 1: A long-time series of measurements were collected comprising 50 matched spectral measurements of each target with each instrument. First, the spectrometers were optimised and dark current measurements were collected. Then measurements were collected following a repeating pattern. First, the tripod arm was positioned over the centre of a white reference panel and a reference measurement was taken. Then the tripod arm was moved over the grey75 target and measurements were collected. Subsequently, grey20 and grass targets were measured before the spectrometer optics were returned to the start of the sequence again. A typical sequence of four sequential measurements took 2 minutes. Stage 1 was complete at solar noon (1200). This stage sought to determine the reproducibility of measurements collected with the different instruments over periods where conditions were changing. Integration speeds for each instrument were as follows:

- ASD FieldSpec Pro – Integration speed was 34 ms
- PP Systems Unispec – Integration speed varied between 5 and 15 ms
- Ocean Optics Vis-NIR – Integration speed varied between 22 and 38 ms
- Ocean Optics NIR Fluorescence – Integration speed varied between 550 and 1000 ms

Stage 2: At 1200, ten measurements were collected in rapid succession of each of the four targets using the simultaneously triggered spectroradiometers. Instrument optimisation and dark current measurements were carried out at the start of the sequence. Here, the tripod arm was not moved between the measurements, i.e. over each target 10 spectra were collected simultaneously with all instruments without moving the arm. The aim of this stage was to determine the short time series repeatability of the four spectrometers, i.e. their noise equivalent delta reflectance characteristics under conditions where there were only very minimal changes in ambient conditions and where spectrometer fore-optics were not moved between measurements of the same target. Integration speeds for each instrument were as follows:

- ASD FieldSpec Pro – Integration speed was 34 ms
- PP Systems Unispec – Integration speed was 8 ms
- Ocean Optics Vis-NIR – Integration speed was 25 ms
- Ocean Optics NIR Fluorescence – Integration speed was 650 ms

#174520 - $15.00 USD Received 22 Aug 2012; revised 2 Nov 2012; accepted 4 Nov 2012; published 7 Jan 2013

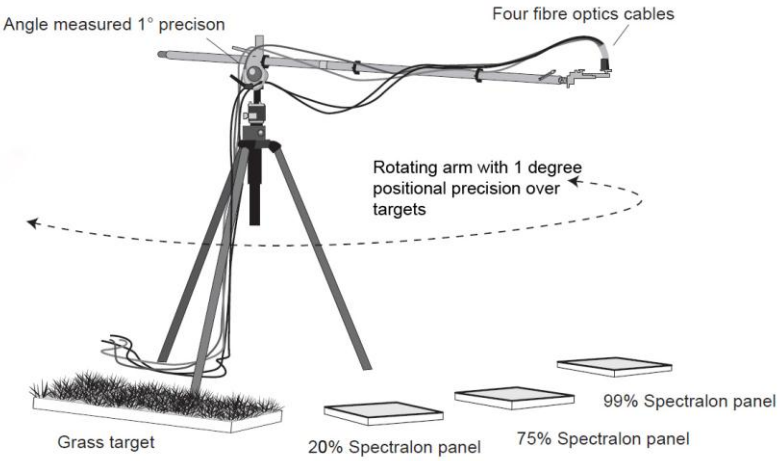

Fig. 1. Experimental field approach.

2.3 Metadata

A range of metadata were collected simultaneously with the experiment. These included:

(a) Full spectrum (350-2500 nm) sky diffuse:global (DG) irradiance ratio data using a SpectraVista SVC HR-1024 spectroradiometer fitted with a 3 inch integrating sphere attachment, with a modified input port to provide an improved cosine response. These data were used to validate the state of the atmosphere during the experiment.

(b) Hemispherical photography at regular intervals using a Nikon CoolPix 4500 camera fitted with a Nikon FC-E8 183° fish eye lens to provide a visual picture of the atmospheric conditions in support of (a).

(c) Microtops hand held sun photometer [14] measurements every minute during the experiment to provide quantification of aerosol optical thickness at the solar disc.

2.4 Correcting for differences in instrument FWHM

Each instrument had a different FWHM (Table 1) and therefore this physical difference in the measurements could not be addressed until the data were post-processed. In order to compare measurements collected with different instruments, radiance spectra acquired with spectrometers having smaller FWHM were degraded to those of the coarsest spectral resolution (10 nm; PP Systems Unispec – see Table 1). The convolution filter was thus applied to ASD and Ocean Optics radiance spectra to degrade them to 10 nm FWHM for inter-comparison.

Assuming that the spectral response function can be approximated by a Gaussian function, the degraded spectra were computed as the convolution of the original spectra with a kernel K computed as a function of the original ($FWHM_o$) and degraded ($FWHM_d$) FWHMs (Eq. (1)) [15, 16]:

$$K = \frac{1}{\sqrt{2\pi}\sqrt{\sigma_d^2 - \sigma_o^2}} \times \exp\left(-\frac{x^2}{2\left(\sigma_d^2 - \sigma_o^2\right)}\right) = \frac{2\sqrt{2\ln 2}}{\sqrt{2\pi}\sqrt{FWHM_d^2 - FWHM_o^2}} \times \exp\left(-\frac{4(\ln 2)\,x^2}{FWHM_d^2 - FWHM_o^2}\right) \quad (1)$$

With $\sigma_{d/o} = \dfrac{FWHM_{d/o}}{2\sqrt{2\ln(2)}}$

#174520 - $15.00 USD Received 22 Aug 2012; revised 2 Nov 2012; accepted 4 Nov 2012; published 7 Jan 2013

3. Results

3.1 Atmospheric conditions

During stage 1 of the experiment atmospheric conditions were clean and relatively stable (Fig. 2). Data from the SVC HR-1024 instrument evidence this (Fig. 2(a)). Across the Vis-NIR spectrum measured by the SVC HR-1024 instrument there is evidence of some wavelength-dependent changes in diffuse-to-global irradiance ratios, with higher ratios (approaching 0.3) at shorter wavelengths, caused by clean sky Rayleigh scattering processes. The lowest DG ratios were measured in the Vis-NIR spectrum around 700 nm (DG = 0.05 (Fig. 2(a)). We have extracted a single time series from Fig. 2(a) corresponding to the measurement times of the data collected during the day, from a channel in the NIR (776 nm) and this is shown in Fig. 2(b). This shows that DG ratios were consistently below 0.2 at 776 nm (Fig. 2(b)) being indicative of very clear conditions (evidenced by hemispherical photos shown in Figs. 2(d) and 2(e)), but that there was a slight upwards trend in DG ratio towards solar noon. This trend would likely have been caused by increased haze around the solar disk as the sun's elevation increased during the day, and due to the appearance of occasional peripheral haze clouds around the edge of the measurement area towards the end of the sequence (Fig. 2(f)). Measurements from the microtops sun photometer (Fig. 2(c)) show a general upwards trend in water vapour concentration in the atmosphere (measured directly at the solar disk) which indicates that the general rise in DG ratios during the course of the experiment was caused by water vapour being mobilised into the atmosphere as the solar elevation increased. During stage 2 of the experiment (from 1200 to the end of the data stream), conditions remained similar to those experienced towards the end of stage 1 (Fig. 2) – i.e. illumination was slightly more unstable than had been experienced earlier in the day but conditions were still optimal for optical remote sensing measurements with DG ratios being less than 1.8 throughout.

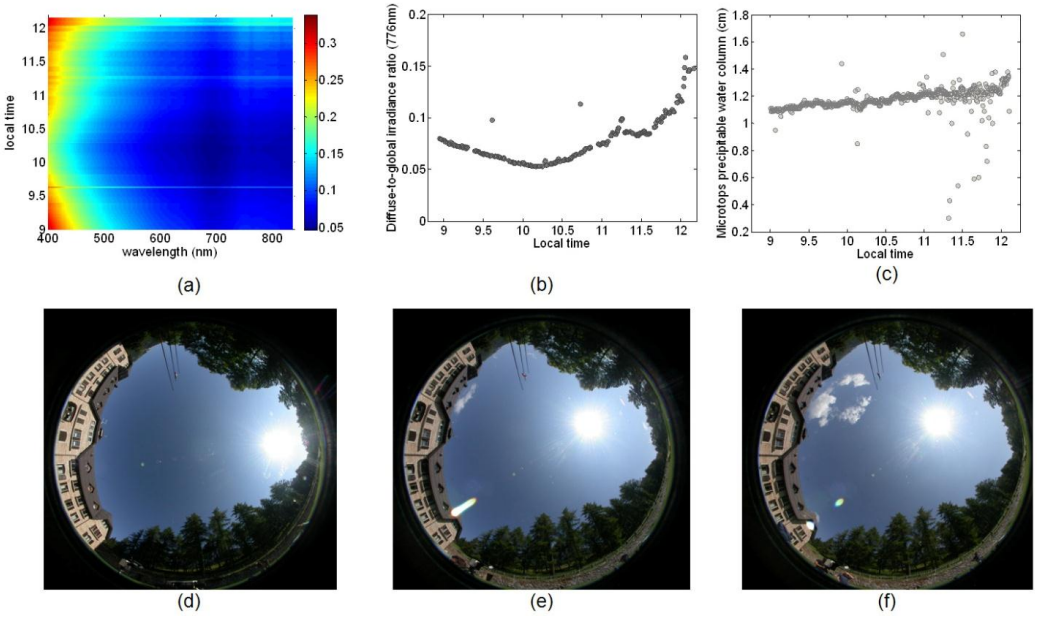

Fig. 2. Atmospheric conditions during the experiment. (a) SVC HR-1024 diffuse-to-global irradiance ratio (expressed as a ratio between 0 and 1) in the visible and NIR range and (b) at a single wavelength (776 nm). (c) Microtops sun photometer water vapour data showing changes during the experimental period. (d-f) Hemispherical photographs of the sky condition over the site, at the (d) beginning; (e) middle; and (f) end of the experiment.

#174520 - $15.00 USD Received 22 Aug 2012; revised 2 Nov 2012; accepted 4 Nov 2012; published 7 Jan 2013

3.2 Stage 1 results

3.2.1 Typical results before FWHM correction

Figure 3 shows an example of the data before instrument-specific FWHM differences were accounted for. Here the mean and SD in the HCRF of the grey20 panel are shown. The main feature of note is the higher channel-to-channel variability in the two Ocean Optics spectroradiometer systems than was seen in the ASD or PP Systems spectroradiometers. This is because of the finer FWHM of the Ocean Optics instruments compared to the PP Systems or ASD spectroradiometers (Table 1). For this reason, we will only present the FWHM-corrected data in the rest of the paper because they permit a more robust assessment of the comparability of the four instruments.

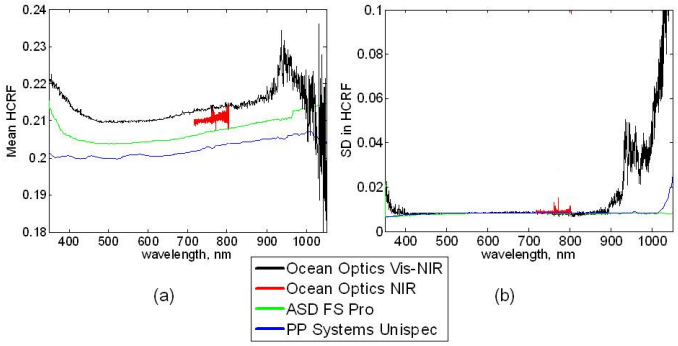

Fig. 3. (a) Mean HCRF and (b) SD in HCRF of the grey20 panel before FWHM correction had been applied in stage 1 of the experiment.

3.2.2 Results after FWHM correction

The results for stage 1 of the experiment after FWHM correction was applied are shown in Fig. 4. The standard deviation (SD) was calculated using all of the data in the sample and hence represents deviation from the mean HCRF for the whole time-series. For the two grey panels, patterns in the SD are very similar with lowest values in the visible region, gradually rising beyond 900 nm in most systems. This is a typical pattern of SD (sometimes reported as "standard uncertainty") that has been reported elsewhere in similar spectroradiometers [12] and is caused by the spectral sensitivity declining towards the extreme measurement limits of silicon photodiode detector arrays. Of all four systems the ASD shows the lowest SD in the range 350-1050 nm, with the PP systems instrument mirroring the ASD most closely in the 400-1000 nm region. The two Ocean Optics instruments show similar SDs for grey20 and grey75 to the PP and ASD systems in the 400-800 nm region, but beyond this range, there is a steep increase in the SD of the Ocean Optics Vis-NIR instrument caused by low radiometric sensitivity at the extremes of its wavelength array.

#174520 - $15.00 USD Received 22 Aug 2012; revised 2 Nov 2012; accepted 4 Nov 2012; published 7 Jan 2013

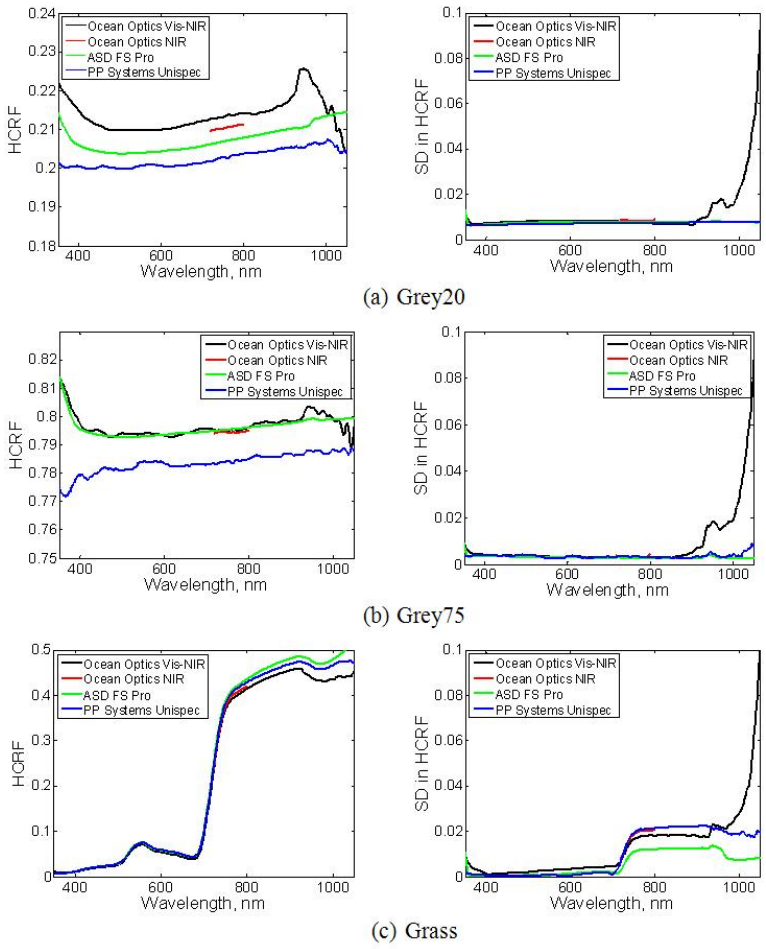

Fig. 4. Mean HCRF plots and standard deviation in HCRF for stage 1 of the experiment showing mean HCRF (left panels) and SD in HCRF (right panels), as represented by the SD in 50 measurements of the target. Data shown are those that have been corrected to normalize the FWHM differences between instruments.

It is important to note the magnitude difference in mean HCRF measured by all four instruments over the two grey panels – Figs. 4(a) and 4(b) show that the different instruments all produced different mean HCRFs of these panels. These magnitude differences could have been caused by spatial non-uniformity in the reflectance properties of the panel, but what is interesting is that the SDs are slightly lower in all instruments for grey75 (SD = 0.003 in the range 400-700 nm) than for grey20 (SD = 0.008 in the range 400-700 nm). Perhaps a more likely explanation for these differences can be found by referring to differences in their bidirectional reflectance response over the time-series of the experiment when solar elevation was changing. Rollin et al. [17] have shown that the carbon added to Spectralon panels to darken them causes a measurable non-Lambertian response, so, for the grey20 panel (which has more carbon added to darken it), the non-Lambertian response may be expected to have a greater impact on the measurement reproducibility than for grey75, which is higher in reflectance and has less carbon added. This helps to explain why SD is larger for the grey20 panel, than for grey75. It is also likely that the slightly different viewing positions for the four fibre-optic cables relative to the positioning of the carbon particles in the panels also caused the instrument-specific differences in mean HCRF shown in Fig. 4, and it is worth

#174520 - $15.00 USD Received 22 Aug 2012; revised 2 Nov 2012; accepted 4 Nov 2012; published 7 Jan 2013

considering that some variability may also have been introduced by temperature-dependent changes in detector sensitivity in the ASD and PP Systems instruments (although we expect this to have had a very small impact).

Note also that the grey75 panel appears to be brighter than its reported reflectance of 75% (Fig. 4(b)), with a HCRF between 0.78 and 0.81 depending on the wavelength viewed, and instrument used, possibly caused by BRDF effects over the time-series.

For the vegetation surface (Fig. 4(c)), the disagreement in mean HCRF between the different instruments was actually much smaller in the visible and NIR than it was for the grey calibration panels. This is evidenced by a lower SD in the range 400-700 nm for the grass target (SD = 0.001 in the range 400-700 nm for the PP systems and ASD instruments; SD = 0.003 for the Ocean Optics Vis-NIR). The SDs for the grass target again show a typical "vegetation spectrum" shape as reported in other work [12] where NIR uncertainties are higher than those measured in visible wavelengths. This can be explained by greater look-to-look variation in the positioning of the spectrometer optics over this spatially and spectrally variable target.

The coefficient of variation ((SD/mean)*100) in HCRF for the three targets allows the data from the three surfaces to be compared more easily (Fig. 5). This corroborates the claim that the grey75 target was the most Lambertian of all three measured (CV<1% in the range 400-1000nm for all three instruments) with no evidence of wavelength-dependent variability either. Grey20 showed limited wavelength-dependent variability but CV was higher (~4%). Grass showed a much higher wavelength-dependency with peaks of ~5% (ASD and PP Systems) and ~12% (Ocean Optics Vis-NIR) in CV around 675 nm and 750 nm (the inflection point for the red edge and top of the red edge respectively).

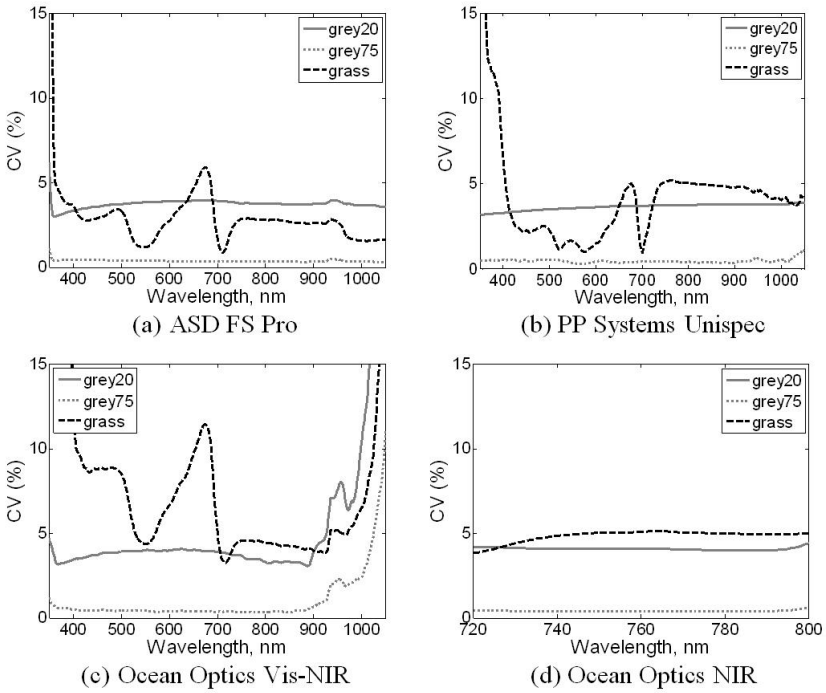

Fig. 5. Coefficient of variation (CV) in HCRF for stage 1 of the experiment for the four spectroradiometers after FWHM correction.

We investigated the hypothesis that BRDF effects were causing these differences in HCRF reproducibility between the three surfaces by simply plotting changes in HCRF against time (Fig. 6) for the ASD FieldSpec Pro. These plots confirm that grey75 is more Lambertian

#174520 - $15.00 USD Received 22 Aug 2012; revised 2 Nov 2012; accepted 4 Nov 2012; published 7 Jan 2013

than grey20 – evidenced by the grey20 plot having an obvious slope with time in both the red (Fig. 6(a)) and NIR (Fig. 6(b)) wavelengths. Grey75 showed no obvious trend in HCRF with time, suggesting it was much more Lambertian in terms of its temporal response. The trends seen in the two wavelengths shown in Fig. 6 were typical across the spectrum for the two grey panels, and were found in all three of the vis-NIR capable instruments. The data for the vegetation target shows two contrasting trends in the red and NIR (Fig. 6). First, vegetation HCRF increases with increasing solar elevation towards noon in the visible part of the spectrum (the trend shown in Fig. 6(a) was typical of trends seen throughout the 400-700 nm region of the spectrum). Secondly, vegetation HCRF decreases with increasing solar elevation towards solar noon in the NIR (Fig. 6(b)). Again these patterns were found in all three of the vis-NIR capable instruments. This suggests a wavelength-dependent time-series trend in BRDF effects for the vegetation target, and is not surprising given the more complex biochemical processes that are indicated by different parts of the vegetation spectrum and the different contributions from the background soil and vegetation components measured by the instrument during the day. At wavelengths shorter than the red-edge foot (e.g. below 700 nm) the vegetation HCRF is usually much lower than that of the background soil, while for wavelengths around the NIR plateau the vegetation is more highly reflective than the soil. The changing SZA in connection with the grass structure has the effect of including or excluding soil contributions. Giving the erectophile structure of grass, the HCRF curve would therefore be expected to be convex, with a maximum HCRF at solar noon for red wavelengths and the opposite for NIR wavelengths, as shown in Fig. 6.

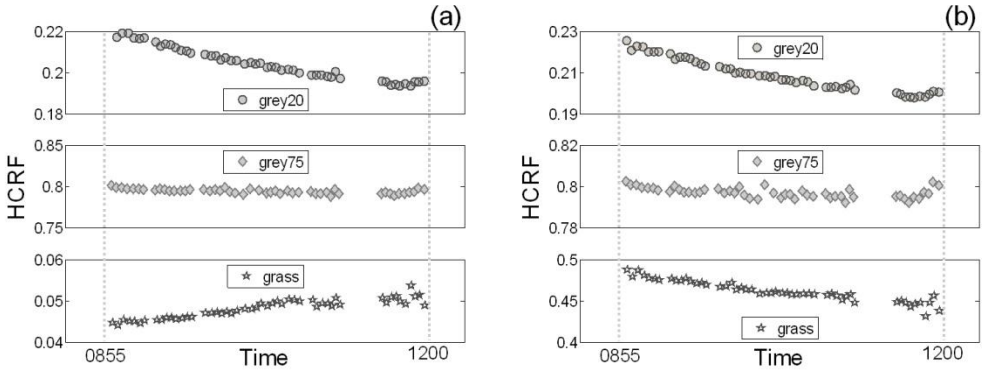

Fig. 6. Changes in HCRF with time at (a) 650 nm and (b) 850 nm measured by the ASD FieldSpec Pro.

3.3 Stage 2 results

Figure 7 shows the SDs for the four targets from stage 2 of the experiment. We have not presented the mean HCRFs because they were very similar between instruments (more so than in stage 1). To evidence this, Table 2 provides mean HCRF data for the 750 nm channel, for the four targets showing that differences in mean HCRF were less than 0.015 for all surfaces. Vegetation showed the highest range in HCRF (0.013) across the four instruments whilst the near-Lambertian optical grade white Spectralon panel and the grey20 panel showed the smallest ranges in HCRF (0.003 and 0.006 respectively). Over the short timescales involved in stage 2 of the experiment, these differences most likely relate to the very slight differences in the measurement support of the four instruments, because as previously explained it was impossible to ensure that the measurement "spot" of all four instruments was completely identical.

#174520 - $15.00 USD Received 22 Aug 2012; revised 2 Nov 2012; accepted 4 Nov 2012; published 7 Jan 2013

Table 2. Mean HCRF for four target surfaces at 750 nm in stage 2 of the experiment (n=10).

Target	ASD FieldSpec Pro	PP Systems Unispec	Ocean Optics Vis-NIR	Ocean Optics NIR Fluorescence	*Range in HCRF*
Vegetation	0.370	0.368	0.357	0.360	*0.013*
Grey 20	0.196	0.197	0.202	0.201	*0.006*
Grey 75	0.785	0.795	0.790	0.790	*0.010*
White	1.004	1.005	1.002	1.002	*0.003*

In Fig. 7 the SDs are lower than those seen in stage 1 of the experiment being quite similar across all four targets with SD typically less than 0.004 in the range 400-850 nm irrespective of the target measured. Again the Ocean Optics systems produced more variable data beyond 850 nm than the ASD or PP systems spectroradiometers. Compared to stage 1, these data show limited variability from one target to another because they do not contain the look-to-look variation imposed by moving the tripod arm between each measurement in the sequence (as was evident in stage 1 of the experiment and shown in Fig. 4). They also contain only minimal HCRF differences caused by changes in solar elevation and atmospheric composition during the experiment – this source of variability was much reduced compared to Stage 1.

The similarity in the SD irrespective of sample type is an indicator that in the range 400-800 nm the four instruments are broadly comparable in terms of the data quality delivered. Such measurements can be readily used to quantify instrument noise equivalent delta reflectance (NEΔρ) [12, 18], and they demonstrate the merits of using a field testing procedure to evaluate the performance of radiometric instruments against each other.

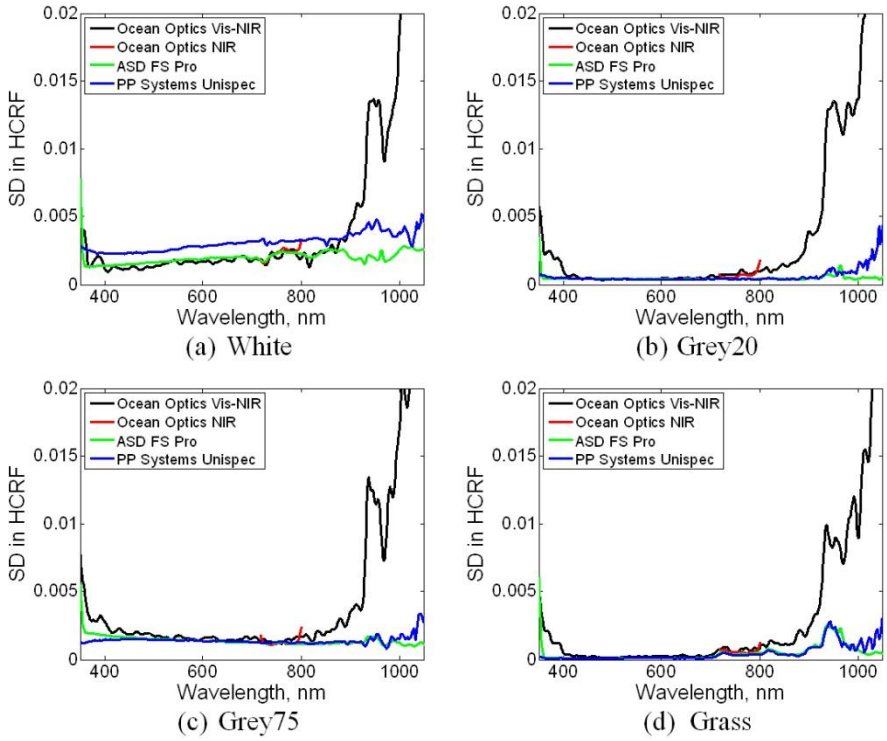

Fig. 7. Standard deviation in HCRF for stage 2 of the experiment for the four targets after FWHM correction.

#174520 - $15.00 USD Received 22 Aug 2012; revised 2 Nov 2012; accepted 4 Nov 2012; published 7 Jan 2013

4. Concluding remarks

A methodology for correcting FWHM differences between instruments considered in this study has been applied before undertaking inter-comparison of data collected by different systems. Using FWHM corrected data, the work has shown that the four instruments produced comparable NEΔρ characteristics (SD < 0.04) in the range 400-800 nm during a short field-based measurement sequence (stage 2) when solar irradiance conditions were stable and when instrument foreoptics were not moved between measurements. Beyond 850 nm the Ocean Optics vis-NIR spectroradiometer showed higher NEΔρ (SD between 0.005 and 0.02) than the other instruments in this wavelength region (typical SD < 0.005) due to a steep decline in its silicon photodiode sensitivity beyond this point. The most important finding from the short time-series experiment is that the four instruments have broadly similar radiometric characteristics in the 400-850 nm measurement range, with typical NEΔρ characteristics showing SD of less than 0.005. This is an important finding because most narrow-band vegetation indices (e.g. PRI [19]) require data in this narrow optical range, and these indices underpin studies of canopy spectral characteristics at eddy covariance sites. This is good news for eddy covariance studies because it shows for the first time that data delivered by lower cost, lightweight spectroradiometers (e.g. Ocean Optics, PP Systems) can provide data of similar precision in this spectral window (e.g. 400-850 nm) to those collected by higher cost, less portable systems (e.g. ASD FieldSpec Pro). The benefit of more lightweight spectroradiometers in eddy covariance settings is that they are more easily modified for unattended deployment [2]. The ASD FieldSpec system on the other hand offers a larger spectral range (350-2500 nm) but is not designed with such applications in mind.

More variable data were found after a longer time-series experiment spanning 2 hours and comprising 50 measurements from each instrument (experiment stage 1). Here, target-specific differences in the SD of the spectral measurements were found, caused by four likely factors:

(a) Look-to-look variations in the targets measured. Despite a very careful experimental design (Fig. 1) and every operational effort to minimize variability, it was impossible to reproduce perfectly the measurement position every time. Our design achieved perfect vertical positional precision, and one degree azimuthal positioning precision. Differences therefore in the azimuthal position of the fibre-optics over the spatially variable targets would have given rise to some spectral variability in HCRF through time.

(b) The design of the instruments also meant that it was impossible to position each spectroradiometer fibre to view the same "spot" on the target and so there was by necessity, less than 3 mm separation between the fibre positions on the rotating tripod arm. Although small, these slight positional differences would have given rise to further variability in the data.

(c) Temporal variation in HCRF caused by surface BRDF responses to changing sun angle and sky irradiance should be considered. The latter effect was strongly surface- and wavelength-dependent. This result points to the need for users of such instruments to consider, and quantify these factors before attributing change in HCRF to "real" factors.

(d) Slight temporal variability in the temperature-dependent sensitivities of the ASD and PP Systems instruments can be considered a possible (but minimal) source of additional variability.

For these reasons, instrument radiometric performance coupled with methodological uncertainty need to be considered in every experiment seeking to utilize such instrumentation to describe changes in surface "reflectance" characteristics.

#174520 - $15.00 USD Received 22 Aug 2012; revised 2 Nov 2012; accepted 4 Nov 2012; published 7 Jan 2013

Acknowledgments

The field experiment described in this paper was undertaken by participants in the EU funded COST Action (ES0903 "Eurospec"; http://cost-es0903.fem-environment.eu/) as part of a Summer School exercise in July 2011. Travel to the field site in Monte Bondone was part-funded by the EU COST action (PI: Loris Vescovo) through travel reimbursement to the Summer School instructors who are the authors of this paper. We are grateful to the participants of the Summer School for their help in setting up the experiment. We also wish to thank PP Systems, who lent Javier Pacheco-Labrador the 2m fibre optic cables used in the experiment and we are grateful to the BIOSPEC project (CGL2008-02301/CLI; http://www.lineas.cchs.csic.es/biospec) funded by the Spanish Ministry of Science and Innovation which has provided funding for Javier Pacheco-Labrador's research.

#174520 - $15.00 USD Received 22 Aug 2012; revised 2 Nov 2012; accepted 4 Nov 2012; published 7 Jan 2013